

Attention-embedded Quadratic Network (Qtention) for Effective and Interpretable Bearing Fault Diagnosis

Jing-Xiao Liao¹, Hang-Cheng Dong¹, Zhi-Qi Sun¹, Jinwei Sun¹, Shiping Zhang^{1*}, Feng-Lei Fan^{2*}

Abstract—Bearing fault diagnosis is of great importance to decrease the damage risk of rotating machines and further improve economic profits. Recently, machine learning, represented by deep learning, has made great progress in bearing fault diagnosis. However, applying deep learning to such a task still faces two major problems. On the one hand, deep learning loses its effectiveness when bearing data are noisy or big data are unavailable, making deep learning hard to implement in industrial fields. On the other hand, a deep network is notoriously a black box. It is difficult to know how a model classifies faulty signals from the normal and the physics principle behind the classification. To solve the effectiveness and interpretability issues, we prototype a convolutional network with recently-invented quadratic neurons. This quadratic neuron empowered network can qualify the noisy and small bearing data due to the strong feature representation ability of quadratic neurons. Moreover, we independently derive the attention mechanism from a quadratic neuron, referred to as qtention, by factorizing the learned quadratic function in analogue to the attention, making the model with quadratic neurons inherently interpretable. Experiments on the public and our datasets demonstrate that the proposed network can facilitate effective and interpretable bearing fault diagnosis.

Index Terms—Bearing fault diagnosis, quadratic convolutional network (QCNN), quadratic attention (qtention).

I. INTRODUCTION

THE reliability of rotating machines such as wind turbines and aircraft engines is a critical issue and must be ensured at all times in the industrial field. Among major mechanical components of a rotating machine, bearings are the most popular source of faults. According to several studies [1], bearing faults are responsible for 40 to 70 percents of electromagnetic drive system failures. Therefore, the diagnosis to bearing faults is of great criticality to improve the availability of rotating machines and further avoid economic loss. A common and viable method to detect bearing faults is analyzing vibration signals that are produced by attaching the measuring instrument to the rotating bearing [2]. Previous

diagnosis works can be divided into two categories: signal processing-based methods vs data-driven methods [3].

Signal processing-based methods usually utilize Fourier transform [4], short-time Fourier transform [5], Hilbert-Huang transform [6], [7], etc. to transform a sequence of a signal into the frequency domain or time-frequency domain. Then, the spectral analysis is conducted to capture the feature of failed faults from the normal. Despite theoretical soundness, these methods suffer from the following weaknesses: 1) Because bearings are always installed in a complex mechanical system, the measured signal is filled with interference from other mechanical components and background noise from the measurement device [1]. This requires a sophisticated and careful design of the denoising model in order to extract various fault characteristics from the complex noise environment. 2) Because different bearing structures and diameters lead to different characteristic frequencies of the faults, the manually-determined parameters are required in performing signal processing-based methods to maximize their diagnosis performance, which is neither intelligent nor scalable due to the complexity of industrial fields [3].

To overcome the above weaknesses, machine learning, particularly deep learning, is widely introduced for bearing fault diagnosis with the promise of big data empowered end-to-end accurate feature discrimination. The past several years have seen a variety of deep learning models developed. Wen *et al.* [8] first folded 1D time-domain signals into 2D images, and then used LeNet-5 as a backbone to classify these images. Concurrently, more studies directly worked on 1D time-domain signals with the help of 1D-CNN [8], [9]. WDCNN adopted a wide convolution kernel in the first layer as the signal extractor for 1D signals and achieved satisfactory results on several bearing fault benchmarks [10]. Due to the outperformance of the WDCNN, more advanced models have been devised based on the WDCNN [11], [12]. Moreover, the attention module was introduced in bearing fault diagnosis because it helps a network focus on fault features and further enhances feature extraction capabilities. Researchers in [11], [13]–[15] inserted a multi-attention module into a 1D-CNN, which not only improves the network’s classification accuracy but also makes the network interpretable.

Despite that deep learning models have made a big stride in bearing fault detection, there are still challenges ahead that need to be addressed. 1) (Effectiveness) Currently, deep

*Shiping Zhang (spzhang@hit.edu.cn) and Feng-Lei Fan (hitfanfenglei@gmail.com) are co-corresponding authors.

¹Jing-Xiao Liao, Hang-Cheng Dong, Zhi-Qi Sun, Jinwei Sun, Shiping Zhang are with School of Instrumentation Science and Engineering, Harbin Institute of Technology, Harbin, China.

²Feng-Lei Fan is with Weill Cornell Medicine, Cornell University, New York City, USA.

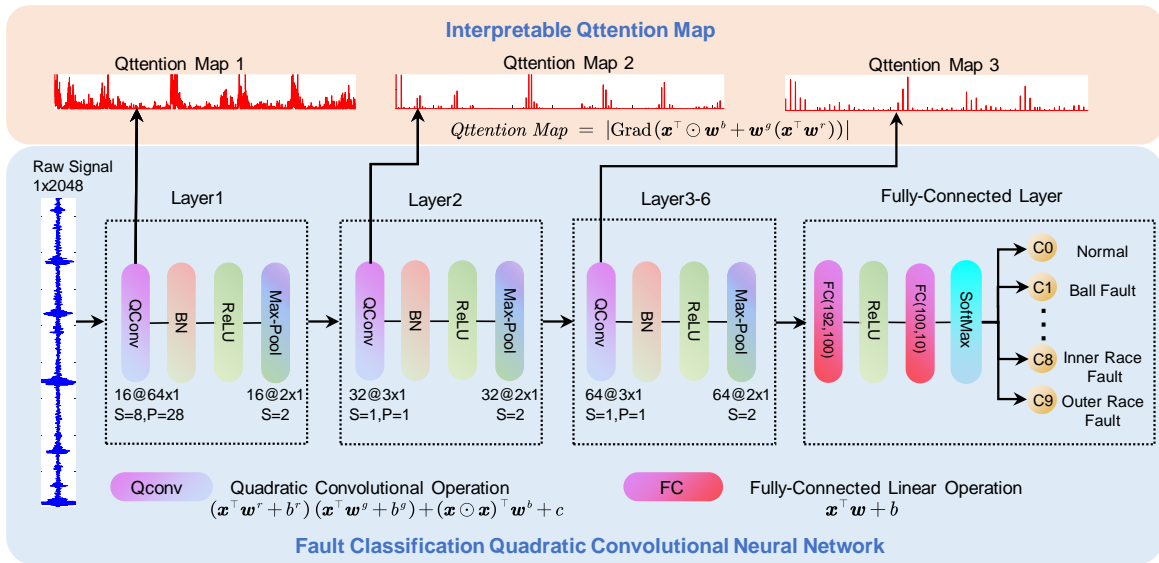


Fig. 1: The proposed quadratic convolutional neural network (QCNN).

learning models can perform superbly, *i.e.*, achieving over 90% accuracy, when the signals are clean or big data are curated. However, when signals are highly corrupted by noise or only small data are available, the performance of deep learning models drops dramatically. The above issue should be accommodated if one wants to implement a deep learning model in industrial fields. 2) (Interpretability) Deep learning, comprising of a series of nonlinear or recursive operations, is notoriously a black box [16]. Due to the lack of interpretability, it is hard to know the physics principle used by a model to pick fault signals out and what changes can be made to further boost the model's diagnosis performance.

To deal with the challenges in effectiveness and interpretability, here we turn our eyes to the quadratic neurons and associated models. Recently, motivated by introducing neuronal diversity in deep learning, a new type of neuron called quadratic neuron [17] was proposed by replacing the inner product in the conventional neuron with a simplified quadratic function. *Why are quadratic neurons promising in solving the effectiveness and interpretability issues?* For the former, it has been empirically and theoretically shown [17], [18] that a quadratic network enjoys a high feature extraction ability. Due to such a character, quadratic models have the potential of qualifying the noisy and small-data bearing diagnosis. For the latter, as our independent methodological finding, the learned quadratic function in a quadratic neuron can induce an attention map through factorization, referred to as *qttenion*, making a quadratic network interpretable. Compared to the classical attention mechanism, which is global and computationally expensive, the qttenion spotlights local fine-grained importance maps and consumes fewer parameters, which is a valuable addition to the attention-based interpretability. In summary, our contributions are twofold:

- We propose a simple and effective model that is made of quadratic neurons for bearing fault diagnosis. The quadratic neurons directly augment the model to outperform other state-of-the-arts in noisy and small data

settings. Different from previous structural modifications, our innovation is at the neuronal level, and is the first work to apply different neurons to bearing fault diagnosis.

- Methodologically, we derive the qttenion mechanism from quadratic neurons, which greatly facilitates the understanding to the model made of quadratic neurons, with an emphasis on the model's physics mechanism when combined with envelope spectrum analysis.

II. METHODOLOGY

A. Quadratic Convolutional Neural Network

Encouraged by the neuronal diversity in a biological neural system, a new type of neuron called quadratic neuron [17] was proposed to promote the neuronal diversity in deep learning. A quadratic neuron [17] integrates two inner products and one power term of the input vector before nonlinear activation. Mathematically, suppose that the input vector is $\mathbf{x} = (x_1, x_2, \dots, x_n)^\top$, the output $f(\mathbf{x}) : \mathbb{R}^n \rightarrow \mathbb{R}$ of a quadratic neuron is

$$\begin{aligned} \sigma(f(\mathbf{x})) &= \sigma\left(\left(\sum_{i=1}^n w_i^r x_i + b^r\right)\left(\sum_{i=1}^n w_i^g x_i + b^g\right) + \sum_{i=1}^n w_i^b x_i^2 + c\right) \\ &= \sigma\left((\mathbf{x}^\top \mathbf{w}^r + b^r)(\mathbf{x}^\top \mathbf{w}^g + b^g) + (\mathbf{x} \odot \mathbf{x})^\top \mathbf{w}^b + c\right), \end{aligned} \quad (1)$$

where $\sigma(\cdot)$ is a nonlinear activation function, \odot denotes the Hadamard product, $\mathbf{w}^r, \mathbf{w}^g, \mathbf{w}^b \in \mathbb{R}^n$ are weight vectors, and $b^r, b^g, c \in \mathbb{R}$ are biases. Superscripts r, g, b are just marks for convenience without special implications.

With the neuronal diversity, we argue that the network design consists of two parts: the neuronal design and the structural design. Figure 1 shows the proposed quadratic convolutional neural network (QCNN). At the neuronal level, we adopt quadratic neurons in hope that they can facilitate bearing diagnosis via the strong feature representation power. Specifically, the QCNN substitutes the conventional convolution with the quadratic convolution operations in convolutional layers. Structurally, we inherit the structure of the WDCNN [10] as

the structure of the proposed model because the WDCNN is a well-established model whose design has been considered by many follow-up studies. This structure stacks 6 CNN blocks and 1 fully-connected layer.

B. Superiority of Representation

The quadratic neurons have the intrinsic enhancement in terms of representation ability, *i.e.*, the enhancement is not due to the increased parameters but the involved nonlinear computation. First, the nonlinear mapping of a conventional neuron is only provided by activation function, whereas a quadratic neuron adds an extra non-linear mapping by using the quadratic aggregation function. As such, a single quadratic neuron can realize XOR logic which is not doable by the conventional neurons unless they are connected into a network. Second, a quadratic neuron is not equivalent to the combination or summation of three conventional neurons. Suppose that the activation function $\sigma(\cdot)$ is ReLU, the combination of conventional neurons can only be a piecewise linear function, but a quadratic neuron is a piecewise polynomial function [18]. As we know, a polynomial spline is better at approximating complicated functions than a linear spline.

Furthermore, Fan *et al.* [17] proved a theorem to demonstrate that a quadratic network is far more powerful to approximate a kind of functions than its conventional counterpart, *i.e.*, a quadratic network can approximate these functions with a polynomial number of neurons, but a conventional network needs an exponential number of neurons to achieve the same level of error. This theorem theoretically provides us a guarantee that a quadratic network is more expressive.

Theorem (Theorem 1 of [17]): Given universal constants $c > 0, C > 0, C' > 0, c_\sigma > 0$, there exists a probability measure μ and a radial function $\tilde{g} : \mathbb{R}^d \rightarrow \mathbb{R}$, with $d > C$ being bounded on $[-2, 2]$ and supporting on $\|\mathbf{x}\| \leq C'\sqrt{d}$. Let f_1 be a one-hidden-layer conventional network, f_2 be a one-hidden-layer quadratic network, the following holds:

1. For any f_1 that has the width at most ce^{cd} , it satisfies

$$\mathbb{E}_{\mathbf{x} \sim \mu}(f_1(\mathbf{x}) - \tilde{g}(\mathbf{x})) \geq c.$$

2. There exists f_2 such that \tilde{g} can be approximated with no more than $C'c_\sigma d^{3.75}$ neurons.

With the quadratic network as a more powerful model, a problem naturally arises: how can we ensure that the model can find a better solution? To address this problem, Fan *et al.* [18] proposed the so-called ReLinear algorithm, where the parameters in a quadratic neuron are initialized as $\mathbf{w}^g = 0, \mathbf{b}^g = 1, \mathbf{w}^b = 0, \mathbf{c} = 0$, and \mathbf{w}^r, b^r follow the normal initialization. Consequently, during the initialization stage, every quadratic neuron in a network degenerates to a conventional neuron. Next, during the training stage, a normal learning rate γ_r is cast for (\mathbf{w}^r, b^r) , and a relatively small learning rate $\gamma_{g,b}$ for $(\mathbf{w}^g, b^g, \mathbf{w}^b, c)$. Under the setting of the ReLinear algorithm, when $\gamma_{g,b} = 0$, the quadratic network turns into the conventional network all the time because the quadratic terms are never updated. Thus, with the ReLinear algorithm, the quadratic network at least performs as well as the conventional network, even if not better. Nevertheless, if $\gamma_{g,b}$ is appropriately set, the quadratic terms participate

in feature learning and should be able to boost superior performance as the theory suggests.

C. Attention-induced Interpretability

The attention module [19] was originally derived for sequence tasks such as natural language processing. Mathematically, given the input signal $\mathbf{x} \in \mathbb{R}^{n \times k}$, the commonly-used scaled dot-product self-attention [20] is formulated as

$$\text{softmax}\left(\mathbf{x}\mathbf{W}^Q(\mathbf{x}\mathbf{W}^K)^\top/\sqrt{d_k}\right)(\mathbf{x}\mathbf{W}^V), \quad (2)$$

where $\mathbf{W}^Q, \mathbf{W}^K, \mathbf{W}^V \in \mathbb{R}^{k \times k'}$ are the projections for the query, key, and value, respectively, and d_k is the scaling factor. The attention that reflects the importance of the input is taken as the following formula from Eq. (2):

$$\text{Att}(\mathbf{x}) = \text{softmax}\left(\mathbf{x}\mathbf{W}^Q(\mathbf{x}\mathbf{W}^K)^\top/\sqrt{d_k}\right). \quad (3)$$

The above attention mechanism is widely adopted in the transformer models [21]. Concurrently, channel and spatial attention modules are developed to adapt the CNN [22]:

$$\begin{aligned} \mathbf{F}' &= \mathbf{M}_c(\mathbf{F}) \odot \mathbf{F} \\ \mathbf{F}'' &= \mathbf{M}_s(\mathbf{F}') \odot \mathbf{F}', \end{aligned} \quad (4)$$

where $\mathbf{F} \in \mathbb{R}^{C \times H \times W}$ denotes an intermediate feature map produced by a convolutional layer, $\mathbf{M}_c \in \mathbb{R}^{C \times 1 \times 1}$ denotes a 1D channel attention map, and $\mathbf{M}_s \in \mathbb{R}^{1 \times H \times W}$ denotes a 2D spatial attention map. Furthermore,

$$\begin{aligned} \mathbf{M}_c(\mathbf{F}) &= \sigma(\text{MLP}(\text{AvgPool}(\mathbf{F})) + \text{MLP}(\text{MaxPool}(\mathbf{F}))) \\ &= \sigma(\mathbf{W}_1(\mathbf{W}_0(\mathbf{F}_{\text{avg}}^c)) + \mathbf{W}_1(\mathbf{W}_0(\mathbf{F}_{\text{max}}^c))) \\ \mathbf{M}_s(\mathbf{F}') &= \sigma(\text{Conv}([\text{AvgPool}(\mathbf{F}'); \text{MaxPool}(\mathbf{F}')])), \end{aligned} \quad (5)$$

where $\sigma(\cdot)$ is the sigmoid function, AvgPool is the average pooling, MaxPool is the max pooling, MLP is the MLP layer, and Conv is the convolution filter. Regardless of the variants, the key of the attention mechanism is to induce an importance map regarding the input that forces the network to discriminatively take advantage of the input information.

Based on such an observation, we find that a quadratic neuron also contains an attention mechanism, referred to as *qtention*, by factorizing the learned quadratic function in analogue to attention. Mathematically, we factorize the expression of a quadratic neuron (Eq. (1)) as follows (we remove constant terms for conciseness):

$$\begin{aligned} &\sigma((\mathbf{x}^\top \mathbf{w}^r + b^r)(\mathbf{x}^\top \mathbf{w}^g + b^g) + (\mathbf{x} \odot \mathbf{x})^\top \mathbf{w}^b + c) \\ &= \sigma(\mathbf{x}^\top \mathbf{w}^g (\mathbf{x}^\top \mathbf{w}^r + b^r) + b^g \mathbf{x}^\top \mathbf{w}^r + b^g b^r + (\mathbf{x} \odot \mathbf{x})^\top \mathbf{w}^b) \\ &= \sigma(\mathbf{x}^\top (\mathbf{w}^g (\mathbf{x}^\top \mathbf{w}^r + b^r)) + \mathbf{x}^\top (\mathbf{w}^r b^g) + \mathbf{x}^\top (\mathbf{x} \odot \mathbf{w}^b)) \\ &= \sigma(\mathbf{x}^\top (\mathbf{x} \odot \mathbf{w}^b + \mathbf{w}^g (\mathbf{x}^\top \mathbf{w}^r + b^r) + \mathbf{w}^r b^g)) \\ &= \sigma(\mathbf{x}^\top (\underbrace{\mathbf{x} \odot \mathbf{w}^b + \mathbf{w}^g \mathbf{x}^\top \mathbf{w}^r}_{\text{qtention}} + \underbrace{\mathbf{w}^g b^r + \mathbf{w}^r b^g}_{\text{bias}})), \end{aligned} \quad (6)$$

where we let

$$\text{RawQtt}(\mathbf{x}) = \mathbf{x}^\top \odot \mathbf{w}^b + \mathbf{w}^g (\mathbf{x}^\top \mathbf{w}^r). \quad (7)$$

We exclude the bias terms $\mathbf{w}^g b^r, \mathbf{w}^r b^g$ because they keep intact for different \mathbf{x} ; therefore, they fall short of serving

as importance scores. Furthermore, we calculate the gradient of $RawQtt(\mathbf{x})$ and take the absolute value to get the final qttention map:

$$Qtt(\mathbf{x}) = |\text{Grad}(RawQtt(\mathbf{x}))|. \quad (8)$$

The reason of doing so is that the gradient can better indicate the trend of the change and further eliminate the common bias, which highlights significant areas of attention weights.

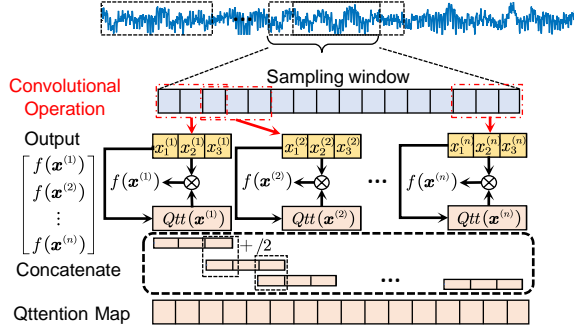


Fig. 2: The workflow of establishing the qttention map for the entire signal in the framework of the convolutional operation.

In a convolutional layer, the qttention is tightly coupled to the convolution operation. Figure 2 illustrates the workflow of establishing the qttention map for the entire signal. Each convolutional kernel is considered to be a single neuron and a convolutional operation is shifting the kernel over the input with a constant stride. At each receptive field, the computation of the convolution kernel follows Eq. (1) and generates a qttention map. The final qttention map for the entire signal is derived by concatenating all qttention maps at local receptive fields. When the stride is smaller than the length of the receptive field, two neighboring receptive fields overlap. Then, we average the qttention scores at the overlapped locations.

Remark 1. What makes the qttention different from the conventional attention module is that the conventional one usually is an independent plug-and-play module, but the qttention is neuron-induced. We summarize that the qttention has the following characteristics:

- (Efficient) The channel and spatial attention compute an element-wise product for the entire input. Moreover, the channel attention module also includes an MLP network. Both the element-wise product for the entire input and the MLP network are computationally heavy. In contrast, the qttention is generated by a convolution operation whose number of weights only scales with the kernel size. In our QCNN, the largest convolution kernel is 1×64 dimension, and therefore the number of qttention weights is at most 192. But the number of parameters in the channel and spatial attention modules is much more.
- (Local) Compared to the typical attention module (Eq. (2)) which is global, the qttention is local. The locality of the qttention is more suitable for bearing fault diagnosis. Usually, the attention module is applied after the signal is divided into several patches. Then, the attention score is assigned to each patch, and the attention map is for the

entire signal but coarse-grained. In contrast, the qttention is associated with the convolution, which emerges at each local receptive field. The locality of the qttention fits the diagnosis because the fault usually presents in the time domain as periodic short-range high-amplitude vibrations.

Remark 2. As an independent methodological finding, we derive the qttention from quadratic neurons. The values of the qttention represent the importance levels of the input \mathbf{x} so that a quadratic network admits a self-explanatory feature extraction capability. This is a unique advantage of using quadratic neurons. In contrast, the conventional neuron doesn't enjoy such a kind of explainability because the linear coefficients are independent of the input, and cannot serve as the attention map. Hence, we argue that a quadratic network is an inherently more interpretable model than a conventional network.

III. EXPERIMENTS

In this section, we use two bearing fault datasets to investigate our proposed model. We first compare the QCNN with other SOTA methods under noisy and small data conditions. The results show that the QCNN outperforms its competitors. Then, aided by the interpretability of qttention maps, we successfully decode the feature extraction process of the proposed model and the physics principle accounting for why the model can achieve good classification performance.

A. Datasets Description

CWRU bearing dataset: This widely-used dataset [23] is collected by Case Western Reserve University Bearing Data Center. Two deep groove ball bearings, 6205-2RS JEM SKF and 6203-2RS JEM SKF, are installed in the fan-end (FE) and drive-end (DE) of the electric motor. Single point defects with a diameter of 7, 14 and 21 mils are injected to outer race, inner race and ball of two bearings using electro-discharge machining. Therefore, this dataset has ten categories: nine types of faulty bearings and one healthy bearing. Specially, four levels (0HP, 1HP, 2HP, 3HP) of load are applied onto the shaft which slightly affects the motor speed (1797r/min, 1772/min, 1750r/min, 1730r/min). Vibration data are collected at two sampling rates: 12kHz and 48kHz for DE bearing faults. In this paper, we use the vibration signal collected at DE side with the 12kHz sampling rate.

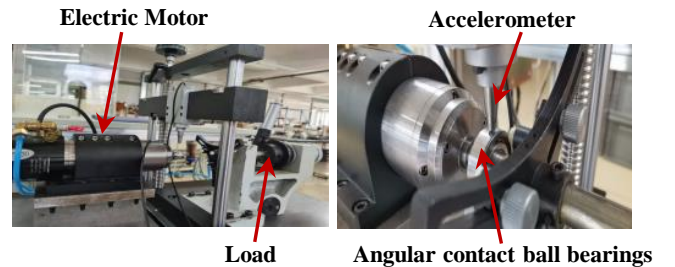


Fig. 3: The instrument for angular contact ball bearing test.

Angular contact ball bearing dataset (Ours): We also prepare a dataset on our own. Figure 3 shows our bearing test rig. We utilize angular contact ball bearings HC7003 for the test.

TABLE I: Ten classes in our dataset. OR and IR denote that the faults appear at outer race and inner race, respectively.

Label	Fault Mode	Label	Fault Mode
C1	Health	C6	OR (Moderate)
C2	Ball cracking (Minor)	C7	OR (Severe)
C3	Ball cracking (Moderate)	C8	IR (Minor)
C4	Ball cracking (Severe)	C9	IR (Moderate)
C5	OR cracking (Minor)	C10	IR (Severe)

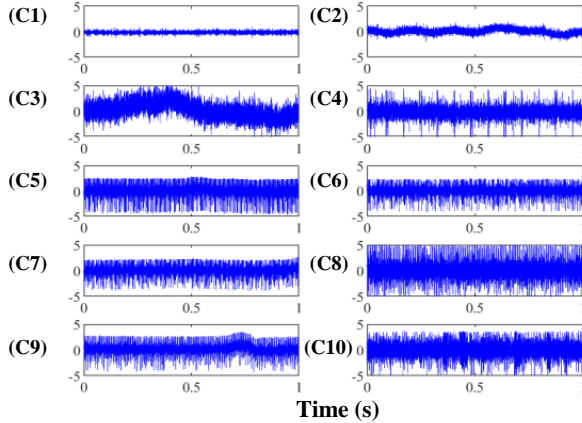


Fig. 4: Raw signals with respect to ten classes of our dataset.

This bearing is for high speed rotating machines compared to a deep groove ball bearing. The accelerometer is directly attached to a bearing to collect vibration signals produced by bearings. Consistent with the CWRU dataset, we inject faults at the outer race (OR), inner race (IR), and ball with three levels (minor, moderate, severe). Table I summaries ten classes of bearings in our dataset. In the test, we choose the constant motor speed (1800 r/min) and use NI USB-6002 to acquire vibration signals with the 12kHz sampling rate. We record 47s of bearing vibration (561,152 points per category). Different from the CWRU dataset, bearing faults here are cracks of the same size but different depths, therefore, the vibration signals between different faults are more similar, making a diagnosis model more difficult to accurately classify. Figure 4 shows the raw signals in the time domain with respect to ten categories of our dataset.

B. Experiment Setup

Data preprocessing. For our dataset, because the original signal is long, we randomly extract short sequences of 2048 numbers from each long sequence 1000 times. As such, we generate a total of 10000 samples. Then, all samples are normalized into $[-1, 1]$. Both datasets are split into training, validation, and test sets with a ratio of 0.5: 0.25: 0.25.

Training settings. The loss function is set to the cross-entropy loss, and we choose the stochastic gradient descent (SGD) [24] optimizer to optimize both networks. To generically compare the performance of all models, we don't add extra training tricks, *e.g.*, weight decay, learning rate decay. We train our model and baseline methods using grid search with the same hyperparameter search space. After searching, we set batch size = 64 for all methods. For the QCNN, the linear terms and quadratic terms are learned with different

learning rates. Let $\gamma_{g,b} = \alpha \cdot \gamma_r$. We search γ_r from $\{0.1, 0.8\}$ and α from $\{10^{-1}, 10^{-2}, 10^{-3}, 10^{-4}, 10^{-5}\}$.

We use the accuracy score to validate the performance of the proposed method, which is defined as where TP, TN, FP, and FN denote the number of true positive, true negative, false positive, and false negative, respectively. Furthermore, we add Gaussian noise into the raw input signal to verify model's performance under noise environments. The signal-to-noise ratio (SNR) is $10 \log_{10}(P_s/P_n)$, where P_s and P_n are average power of the signal and noise.

All experiments are conducted in Windows 10 with an Intel i9 10900k CPU at 3.70 GHz and one NVIDIA RTX 3080Ti 12GB GPU. Our code is written in Python 3.8 with PyTorch, an open-source deep learning framework.

C. Classification Performance

i) The bearing signal is interfered with by other mechanical components and background noise from the measurement device, therefore, the noise-resistant capability of deep learning models is critical to the bearing fault diagnosis. ii) Currently, the bearing fault data are not easy to acquire in practice because the machines most time operate normally. Therefore, whether the model is competent for small data is important. Based on these two real needs, we conduct experiments to verify the classification performance of the proposed model under noisy and small data settings. We compare our method with other SOTA methods, DCA-BiGRU [25], AResNet [26], RNN-WDCNN [12], MA1DCNN [11], WDCNN [10]. Because codes of all these counterpart models are publicly available, we replicate them by their code and utilize the same data preprocessing. Table III summarizes the sizes, #FLOPS, and inference time of all models. Compared to competitors, the QCNN has a relatively small model size, low computational complexity, and short inference time. Note that introducing quadratic neurons in convolutional layers only increases the number of parameters moderately, because the number of parameters in fully-connected layers takes up a high percentage of the WDCNN.

TABLE III: The summary of compared models properties. Time is the elapsed time to infer 1000 samples for each model.

Model	Size	#FLOPS	Inference Time
DCA-BiGRU	626KB	42.4M	4.5977s
AResNet	10.67MB	260.4M	14.7547s
RNN-WDCNN	4407KB	54.3M	5.1949s
MA1DCNN	4172KB	299.7M	5.5341s
WDCNN	284KB	1.6M	0.1925s
QCNN	642KB	4.7M	0.3581s

Performance on noisy data: We set seven noise levels. The results are shown in Table II. All results are the average and std of ten runs. We draw the following highlights from Table II. First, for all datasets and SNR conditions, the QCNN outperforms its competitors in terms of average accuracy. In particular, on our and CWRU-1HP datasets, the average accuracy of QCNN is about 2% higher than the second-best method and 4% higher than the third. Although in some cases where the QCNN is not the best, it ranks second and

admits a small gap to the first place. Therefore, we conclude that the QCNN is a versatile model that consistently delivers competitive performance at various noise levels.

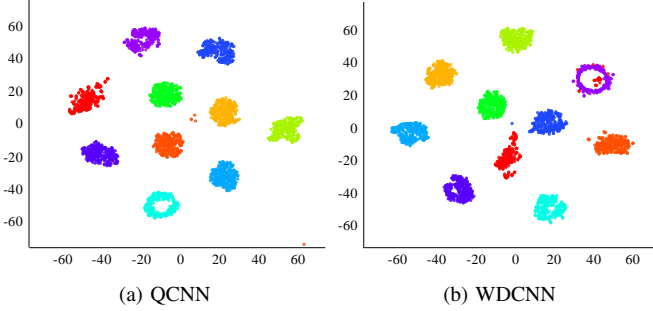


Fig. 5: The t-SNE results of features produced by the last convolutional layers of QCNN and WDCNN on our dataset.

Second, in most cases, the QCNN outcompetes WDCNN. Particularly, the QCNN leads by a large margin on severely noisy signals, *e.g.*, in SNR = -6dB CWRU-1HP dataset, the average accuracy of the QCNN is 4.4% higher than the WDCNN. Since the QCNN and WDCNN share the same structure, it confirms that a quadratic neuron is a simple and effective way of augmenting a network’s performance. To further compare what the QCNN and WDCNN learn from data, we use t-SNE [27] to visualize output features of the last convolutional layers of the QCNN and WDCNN. As shown in Figure 5, different colors denote different categories of bearings. Although both models exhibit promising feature extraction capabilities, evidenced by discernible clusters of 10 categories of data, the QCNN shows better feature discriminatory ability. For example, the purple cluster in the result of the WDCNN

is contaminated by red points, but the purple and red clusters are well separated in the result of the QCNN.

TABLE IV: The average accuracy of all models on small samples. The bold-faced numbers are the best. The underline numbers are the second-best.

	Train Sample	250	500	1000	2500	Average
Ours	DCA-BiGRU	0.3240	0.6240	0.7166	0.7387	0.6008
	AResNet	0.6648	0.6320	0.7250	0.7627	0.6961
	RNN-WDCNN	0.1864	0.2768	0.3794	0.5929	0.3589
	MA1DCNN	0.4832	0.5056	0.6758	0.6897	0.5886
	WDCNN	0.4880	0.6440	0.6740	0.7040	0.6275
	QCNN	<u>0.5680</u>	<u>0.6400</u>	<u>0.7080</u>	<u>0.7240</u>	<u>0.6600</u>
CWRU -0HP	DCA-BiGRU	0.4288	0.7400	0.8110	0.8423	0.7055
	AResNet	0.6960	0.7712	0.8042	0.7865	0.7645
	RNN-WDCNN	0.2624	0.3860	0.5682	0.9004	0.5293
	MA1DCNN	<u>0.7752</u>	<u>0.8860</u>	0.8792	0.9193	<u>0.8649</u>
	WDCNN	0.7520	0.8360	0.8800	0.9264	0.8486
	QCNN	0.8240	0.8920	0.8860	0.9352	0.8843
CWRU -1HP	DCA-BiGRU	0.6304	0.7360	0.8152	0.8409	0.7556
	AResNet	0.7560	0.7828	0.8226	0.8130	0.7936
	RNN-WDCNN	0.2208	0.3772	0.5572	0.9402	0.5239
	MA1DCNN	0.7440	0.8540	0.8830	0.9390	0.8550
	WDCNN	0.8160	0.8880	0.9140	0.9480	0.8915
	QCNN	0.8560	0.8920	0.9240	0.9488	0.9052
CWRU -2HP	DCA-BiGRU	0.6232	0.7560	0.8456	0.8762	0.7752
	AResNet	0.7800	0.8036	0.8200	0.8459	0.8124
	RNN-WDCNN	0.2608	0.3552	0.5826	0.9675	0.5415
	MA1DCNN	<u>0.8256</u>	0.8992	0.9606	0.9685	<u>0.9135</u>
	WDCNN	0.7680	0.9200	0.9380	0.9648	0.8977
	QCNN	0.8160	0.9280	0.9440	0.9720	0.9150
CWRU -3HP	DCA-BiGRU	0.5184	0.7556	0.8304	0.8602	0.7411
	AResNet	0.7312	0.8208	0.8390	0.8405	0.8079
	RNN-WDCNN	0.2344	0.3916	0.5390	0.9176	0.5207
	MA1DCNN	0.8144	0.8808	0.9088	0.9304	0.8836
	WDCNN	0.8160	0.9120	0.9220	0.9592	0.9023
	QCNN	0.8560	0.9280	0.9380	0.9600	0.9205

Performance on small data: Here, we test if the QCNN can deliver satisfactory performance when big data are not available. The number of samples in the training set is set to 250, 500, 1000, and 2500, respectively. The random noise level is SNR = 0dB. The classification results are shown in Table

TABLE II: The average accuracy of all compared methods on noisy data. The bold number denotes the best performance.

	SNR	-6	-4	-2	0	2	4	6	Average
Ours	DCA-BiGRU	0.3305±0.0087	0.4742±0.0094	0.6382±0.0105	0.7442±0.0086	0.8479±0.0045	0.8896±0.0050	0.9242±0.0030	0.6927±0.2073
	AResNet	0.3705±0.0073	0.4903±0.0106	0.6642±0.0076	0.8012±0.0075	0.8807±0.0048	0.9300±0.0051	0.9512±0.0048	0.7269±0.2096
	RNN-WDCNN	0.3598±0.0264	0.4786±0.0521	0.5922±0.0801	0.6660±0.1026	0.7224±0.1290	0.7628±0.1378	0.8013±0.1434	0.6268±0.1483
	MA1DCNN	0.3467±0.0235	0.4872±0.0517	0.5914±0.0842	0.7717±0.1152	0.8305±0.1122	0.8718±0.1030	0.8644±0.1122	0.6805±0.1920
	WDCNN	0.3940±0.0044	0.5148±0.0026	0.6308±0.0079	0.7308±0.0024	0.8444±0.0052	0.8876±0.0092	0.9288±0.0084	0.7045±0.1859
	QCNN	0.4244±0.0013	0.5348±0.0087	0.6892±0.0020	0.8356±0.0033	0.8728±0.0082	0.9192±0.0007	0.9512±0.0061	0.7467±0.1880
CWRU -0HP	DCA-BiGRU	0.6308±0.0065	0.7164±0.0070	0.7801±0.0079	0.8572±0.0045	0.8987±0.0065	0.9480±0.0035	0.9709±0.0024	0.8288±0.0899
	AResNet	0.6121±0.0060	0.6925±0.0044	0.7712±0.0065	0.8429±0.0073	0.9106±0.0065	0.9557±0.0029	0.9785±0.0033	0.8234±0.1277
	RNN-WDCNN	0.5804±0.0059	0.7274±0.0085	0.8876±0.0070	0.9549±0.0057	0.9893±0.0018	0.9938±0.0010	0.9926±0.0015	0.8751±0.1493
	MA1DCNN	0.6954±0.0069	0.7435±0.0071	0.8674±0.0052	0.9319±0.0048	0.9597±0.0025	0.9749±0.0028	0.9816±0.0021	0.8792±0.1077
	WDCNN	0.6652±0.0056	0.7736±0.0094	0.8712±0.0022	0.9420±0.0032	0.9836±0.0056	0.9952±0.0084	0.9992±0.0003	0.8900±0.1189
	QCNN	0.7112±0.0087	0.7992±0.0084	0.8928±0.0051	0.9576±0.0064	0.9852±0.0052	0.9964±0.0016	0.9996±0.0005	0.9060±0.1038
CWRU -1HP	DCA-BiGRU	0.6374±0.0065	0.7176±0.0057	0.7901±0.0064	0.8880±0.0050	0.9418±0.0032	0.9751±0.0026	0.9784±0.0022	0.8818±0.0975
	AResNet	0.6133±0.0054	0.7046±0.0070	0.7887±0.0043	0.8732±0.0046	0.9268±0.0039	0.9684±0.0032	0.9894±0.0016	0.8378±0.1308
	RNN-WDCNN	0.5854±0.0079	0.7422±0.0062	0.8768±0.0050	0.9658±0.0030	0.9776±0.0022	0.9827±0.0019	0.9846±0.0020	0.8714±0.1434
	MA1DCNN	0.7308±0.0086	0.8286±0.0061	0.9047±0.0047	0.9622±0.0027	0.9773±0.0027	0.9853±0.0019	0.9933±0.0016	0.9117±0.0916
	WDCNN	0.6968±0.0051	0.7268±0.0091	0.8860±0.0017	0.9228±0.0056	0.9812±0.0036	0.9792±0.0046	0.9912±0.0007	0.8834±0.1142
	QCNN	0.7080±0.0084	0.8144±0.0040	0.8992±0.0035	0.9624±0.0062	0.9872±0.0078	0.9940±0.0079	0.9964±0.0071	0.9323±0.1023
CWRU -2HP	DCA-BiGRU	0.6622±0.0055	0.7477±0.0059	0.8214±0.0051	0.9148±0.0042	0.9536±0.0030	0.9719±0.0024	0.9914±0.0019	0.8661±0.0876
	AResNet	0.6098±0.0062	0.7208±0.0050	0.8191±0.0059	0.8987±0.0041	0.9550±0.0046	0.9851±0.0020	0.9961±0.0010	0.8549±0.1353
	RNN-WDCNN	0.6790±0.0079	0.8142±0.0051	0.9322±0.0052	0.9816±0.0020	0.9972±0.0009	0.9982±0.0006	0.9999±0.0002	0.9146±0.1143
	MA1DCNN	0.7587±0.0065	0.8552±0.0083	0.9362±0.0052	0.9747±0.0038	0.9906±0.0017	0.9970±0.0010	0.9991±0.0005	0.9302±0.0844
	WDCNN	0.7192±0.0033	0.8372±0.0029	0.9076±0.0052	0.9780±0.0030	0.9908±0.0087	0.9984±0.0044	1.0000±0.0000	0.9187±0.0987
	QCNN	0.7632±0.0095	0.8516±0.0066	0.9352±0.0060	0.9796±0.0063	0.9964±0.0018	1.0000±0.0000	1.0000±0.0000	0.9323±0.0850
CWRU -3HP	DCA-BiGRU	0.6653±0.0039	0.7388±0.0071	0.8328±0.0085	0.8967±0.0069	0.9528±0.0037	0.9806±0.0022	0.9925±0.0020	0.8656±0.0898
	AResNet	0.6311±0.0069	0.7244±0.0088	0.8124±0.0081	0.8962±0.0043	0.9634±0.0025	0.9917±0.0017	0.9989±0.0006	0.8597±0.1312
	RNN-WDCNN	0.6325±0.0085	0.8094±0.0073	0.9419±0.0039	0.9864±0.0021	0.9988±0.0006	0.9999±0.0001	1.0000±0.0000	0.9099±0.1299
	MA1DCNN	0.7463±0.0083	0.8391±0.0046	0.9292±0.0054	0.9747±0.0030	0.9890±0.0029	0.9945±0.0014	0.9995±0.0006	0.9246±0.0897
	WDCNN	0.7240±0.0085	0.8264±0.0048	0.9068±0.0037	0.9660±0.0038	0.9968±0.0024	0.9988±0.0016	1.0000±0.0000	0.9170±0.0985
	QCNN	0.7396±0.0093	0.8444±0.0046	0.9268±0.0043	0.9756±0.0014	0.9952±0.0027	1.0000±0.0000	1.0000±0.0000	0.9259±0.0923

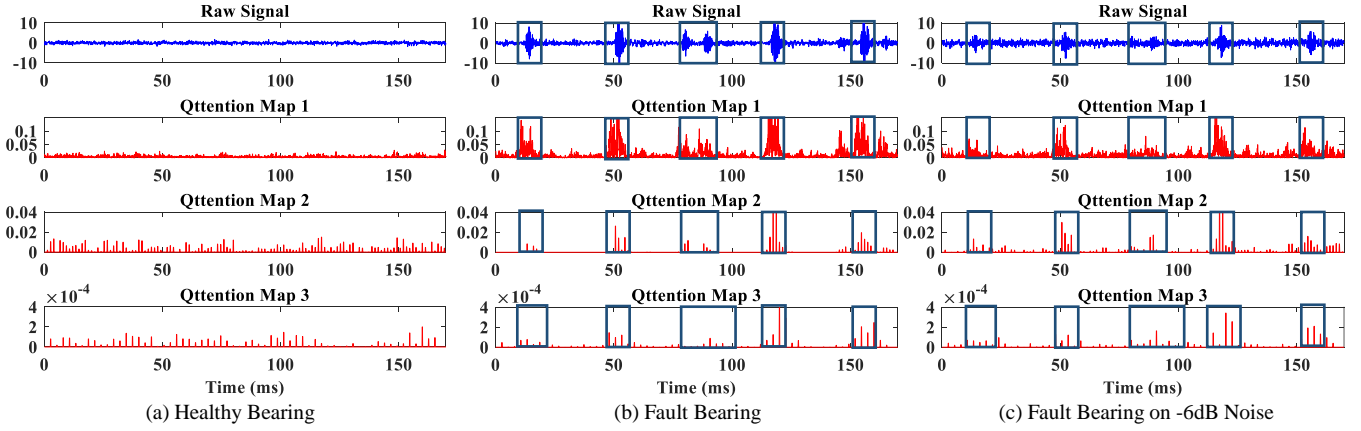


Fig. 6: Three convolutional layers' qtention maps on CWRU IHP. From shallow to deep, the network gradually intensifies its focus on the strongest vibration features.

IV. First, in terms of the average accuracy, the QCNN is the best performer on four CWRU datasets and the second-best performer on our dataset. The QCNN presents a fairly stable performance in different data sizes. Although the QCNN is not the best on our dataset (surpassed by AResNet), it is still a competitive model considering that the model complexity of AResNet is far larger than the QCNN. Second, regarding the extremely small data size (250 training samples), the QCNN shows a great advantage over the WDCNN. In particular, on CWRU-0HP datasets, the average accuracy of the QCNN is 7.2% higher than that of the WDCNN, which confirms that the quadratic neuron possesses a powerful feature extraction capability and is more scalable to small data.

D. Interpretability of Qtention

Interpretability in time domain. Qtention informs what local information a quadratic convolutional layer highlights and the flow of important information across layers. Here, we compute qtention maps from the earlier three quadratic convolutional layers for healthy, faulty, and noisy faulty bearing signals. Because each convolutional layer is followed by a max-pooling layer, the lengths of signals, as well as the corresponding qtention maps, become short. So at the second and third layers, we need to interpolate the attention map to the same dimension of the input. Figure 6 showcases the qtention maps of three signals, where a higher value of qtention means higher importance. First, comparing healthy bearing and faulty bearing, qtention values of the healthy bearing are lower, suggesting that the QCNN pays more attention to the faulty signal. Second, for faulty bearing, the qtention shares a similar trend with the raw signal. All high-magnitude sequences, where the faulty area might be contacted to generate a severe vibration, are captured. As the layer goes deep, the attention to key faulty sequences retains. At last, in regards to the noisy faulty bearing signal, the qtention map can still attend the faulty positions even when the noise almost dominates the raw signal. Moreover, the qtention map of the third convolutional layer keeps similar features to that of the noiseless faulty bearing. This phenomenon accounts for why the QCNN can maintain good performance for noisy signals; the QCNN can consistently acquire useful features even if the signal is noisy.

Interpretability in envelope spectrum. The bearing vibration signal is mixed with multiple frequency components. The sign of a bearing defect is a significant impulse in the frequency domain (the corresponding frequency is called the characteristic frequency). While in the low-frequency domain, there exist the shaft frequency and its harmonics. We are curious to the questions: Does the QCNN really learn features of bearing defects? or does the QCNN just follow those signals with high magnitude and obscure defect signals and shaft signals? To resolve this question, we validate the envelope spectrum of the qtention map of the first convolutional layer by considering the physics principle of bearing defect vibration signals.

The characteristic frequency of bearing defects is caused by balls passing through defect points. Given that n , d , and D are the number of balls, the ball diameter, and the bearing pitch diameter, f_r is shaft speed, and ϕ is the angle of the load from the radial plane, the characteristic frequencies of bearing defects obey the following equations:

$$\begin{cases} f_{\text{BPFO}} = \frac{nf_r}{2} \left(1 - \frac{d}{D} \cos \phi\right) \\ f_{\text{BPFI}} = \frac{nf_r}{2} \left(1 + \frac{d}{D} \cos \phi\right) \\ f_{\text{FTF}} = \frac{f_r}{2} \left(1 - \frac{d}{D} \cos \phi\right) \\ f_{\text{BSF}} = \frac{Df_r}{2d} \left(1 - \left(\frac{d}{D} \cos \phi\right)^2\right), \end{cases} \quad (9)$$

where f_{BPFO} , f_{BPFI} is the ball pass frequency of the outer race and inner race, f_{FTF} is the fundamental train frequency (cage speed), and f_{BSF} is the ball spin frequency [28], [29].

Hilbert-Huang transform (HHT) is a powerful technique to analyze non-stationary signals [28]. By extracting the envelope of the signal through HHT and calculating its frequency spectrum, the characteristic frequencies of the non-stationary signal can be clearly observed [6]. In [30] the characteristic frequencies of faults in the CWRU dataset are computed, here we adopt those computations. Figure 7 shows the envelope spectra of the raw signals and qtention maps. We use f_c to uniformly represent f_{BPFO} , f_{BPFI} , f_{BSF} for simplicity. First, both the envelope spectra of the outer race defect and inner race defect signals exhibit significant shaft frequency and characteristic frequencies, but the characteristic frequency of ball defects is hard to find because the ball is accompanied by spinning and rolling during motion. Second, by comparing the

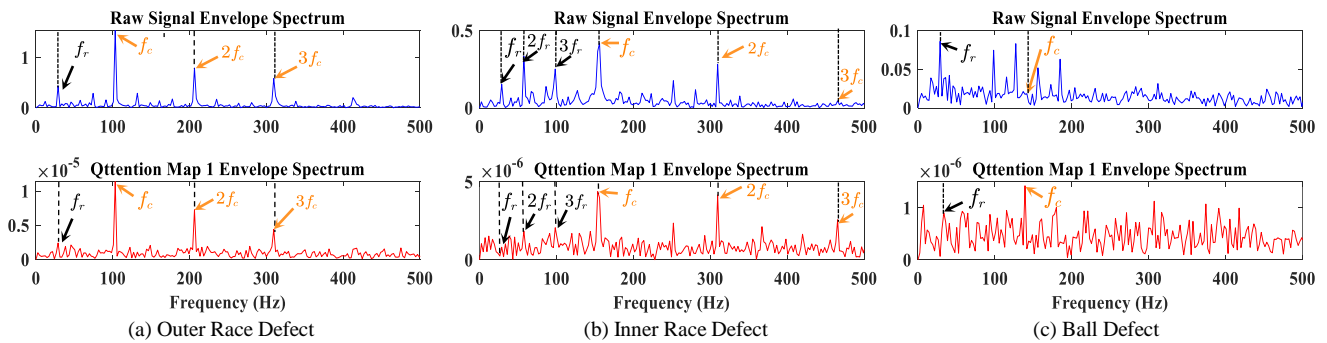


Fig. 7: The envelope spectra (frequency spectrum of the Hilbert-Huang transform) of the raw signals and the attention maps. f_r denotes shaft characteristic frequency, f_c denotes characteristic frequency of different defects.

envelope spectra of the raw signal and the attention map, we find that the QCNN favors bearing fault characteristics over the shaft. For the outer race defect, f_c , $2f_c$, and $3f_c$ are maintained while the shaft frequency is suppressed. For the inner race, f_c and $2f_c$ are maintained, while $3f_c$ are extracted from the raw signal. For ball defects, the f_c element is highly attended, whereas the shaft frequency is moderately attended. We argue that the QCNN indeed learns faulty features via working as an adaptive band-pass filter for different fault modes. At last, regarding the ball defect signal, when the characteristic frequency of the fault is interfered with by signals in similar frequency bands, the QCNN can still accurately identify the characteristic frequency f_c , which confirms that the QCNN has a powerful feature extraction capability.

IV. CONCLUSIONS

In this article, we have proposed a convolutional network made of recently-developed quadratic neurons for the end-to-end time-domain bearing fault diagnosis. Moreover, not only the proposed quadratic convolutional network can have competitive results on either noisy or small data, but also we have independently derived that a quadratic neuron inherently contains an attention mechanism, referred to as attention. Furthermore, we have utilized the attention map to interpret the features learned by the proposed quadratic model in both time and frequency domains and elucidate the physics principle behind. In the future, more efforts are required to refine the attention mechanism and find real-world applications. We will share our code after this manuscript is published.

REFERENCES

- [1] A. H. Bonnett and C. Yung, "Increased efficiency versus increased reliability," *IEEE Industry Applications Magazine*, vol. 14, no. 1, pp. 29–36, 2008.
- [2] P. McFadden and J. Smith, "Model for the vibration produced by a single point defect in a rolling element bearing," *Journal of sound and vibration*, vol. 96, no. 1, pp. 69–82, 1984.
- [3] Y. Ding, J. Zhuang, P. Ding, and M. Jia, "Self-supervised pretraining via contrast learning for intelligent incipient fault detection of bearings," *Reliability Engineering & System Safety*, vol. 218, p. 108126, 2022.
- [4] S. E. Pandarakone, M. Masuko, Y. Mizuno, and H. Nakamura, "Deep neural network based bearing fault diagnosis of induction motor using fast fourier transform analysis," in *2018 IEEE energy conversion congress and exposition (ECCE)*. IEEE, 2018, pp. 3214–3221.
- [5] H. Gao, L. Liang, X. Chen, and G. Xu, "Feature extraction and recognition for rolling element bearing fault utilizing short-time fourier transform and non-negative matrix factorization," *Chinese Journal of Mechanical Engineering*, vol. 28, no. 1, pp. 96–105, 2015.
- [6] V. Rai and A. Mohanty, "Bearing fault diagnosis using fft of intrinsic mode functions in hilbert–huang transform," *Mechanical systems and signal processing*, vol. 21, no. 6, pp. 2607–2615, 2007.
- [7] S. Osman and W. Wang, "A morphological hilbert-huang transform technique for bearing fault detection," *IEEE Transactions on Instrumentation and Measurement*, vol. 65, no. 11, pp. 2646–2656, 2016.
- [8] L. Wen, X. Li, L. Gao, and Y. Zhang, "A new convolutional neural network-based data-driven fault diagnosis method," *IEEE Transactions on Industrial Electronics*, vol. 65, no. 7, pp. 5990–5998, 2017.
- [9] M. Zhao, S. Zhong, X. Fu, B. Tang, and M. Pecht, "Deep residual shrinkage networks for fault diagnosis," *IEEE Transactions on Industrial Informatics*, vol. 16, no. 7, pp. 4681–4690, 2019.
- [10] W. Zhang, G. Peng, C. Li, Y. Chen, and Z. Zhang, "A new deep learning model for fault diagnosis with good anti-noise and domain adaptation ability on raw vibration signals," *Sensors*, vol. 17, no. 2, p. 425, 2017.
- [11] H. Wang, Z. Liu, D. Peng, and Y. Qin, "Understanding and learning discriminant features based on multiattention 1dcnn for wheelset bearing fault diagnosis," *IEEE Transactions on Industrial Informatics*, vol. 16, no. 9, pp. 5735–5745, 2019.
- [12] A. Shenfield and M. Howarth, "A novel deep learning model for the detection and identification of rolling element-bearing faults," *Sensors*, vol. 20, no. 18, p. 5112, 2020.
- [13] X. Li, W. Zhang, and Q. Ding, "Understanding and improving deep learning-based rolling bearing fault diagnosis with attention mechanism," *Signal processing*, vol. 161, pp. 136–154, 2019.
- [14] Z.-b. Yang, J.-p. Zhang, Z.-b. Zhao, Z. Zhai, and X.-f. Chen, "Interpreting network knowledge with attention mechanism for bearing fault diagnosis," *Applied Soft Computing*, vol. 97, p. 106829, 2020.
- [15] H. Wang, J. Xu, R. Yan, C. Sun, and X. Chen, "Intelligent bearing fault diagnosis using multi-head attention-based cnn," *Procedia Manufacturing*, vol. 49, pp. 112–118, 2020.
- [16] Q.-s. Zhang and S.-C. Zhu, "Visual interpretability for deep learning: a survey," *Frontiers of Information Technology & Electronic Engineering*, vol. 19, no. 1, pp. 27–39, 2018.
- [17] F. Fan, J. Xiong, and G. Wang, "Universal approximation with quadratic deep networks," *Neural Networks*, vol. 124, pp. 383–392, 2020.
- [18] F.-L. Fan, M. Li, F. Wang, R. Lai, and G. Wang, "Expressivity and trainability of quadratic networks," *arXiv preprint*, 2021.
- [19] S. Chaudhari, V. Mithal, G. Polatkan, and R. Ramanath, "An attentive survey of attention models," *ACM Transactions on Intelligent Systems and Technology (TIST)*, vol. 12, no. 5, pp. 1–32, 2021.
- [20] M.-T. Luong, H. Pham, and C. D. Manning, "Effective approaches to attention-based neural machine translation," *arXiv preprint arXiv:1508.04025*, 2015.
- [21] Z. Liu, Y. Lin, Y. Cao, H. Hu, Y. Wei, Z. Zhang, S. Lin, and B. Guo, "Swin transformer: Hierarchical vision transformer using shifted windows," in *Proceedings of the IEEE/CVF International Conference on Computer Vision*, 2021, pp. 10012–10022.
- [22] S. Woo, J. Park, J.-Y. Lee, and I. S. Kweon, "Cbam: Convolutional block attention module," in *Proceedings of the European conference on computer vision (ECCV)*, 2018, pp. 3–19.
- [23] D. Neupane and J. Seok, "Bearing fault detection and diagnosis using case western reserve university dataset with deep learning approaches: A review," *IEEE Access*, vol. 8, pp. 93 155–93 178, 2020.
- [24] L. Bottou, "Stochastic gradient descent tricks," in *Neural networks: Tricks of the trade*. Springer, 2012, pp. 421–436.
- [25] X. Zhang, C. He, Y. Lu, B. Chen, L. Zhu, and L. Zhang, "Fault diagnosis for small samples based on attention mechanism," *Measurement*, vol. 187, p. 110242, 2022.

-
- [26] Z. Zhuang, H. Lv, J. Xu, Z. Huang, and W. Qin, "A deep learning method for bearing fault diagnosis through stacked residual dilated convolutions," *Applied Sciences*, vol. 9, no. 9, 2019. [Online]. Available: <https://www.mdpi.com/2076-3417/9/9/1823>
- [27] L. Van der Maaten and G. Hinton, "Visualizing data using t-sne." *Journal of machine learning research*, vol. 9, no. 11, 2008.
- [28] R. B. Randall and J. Antoni, "Rolling element bearing diagnostics—a tutorial," *Mechanical systems and signal processing*, vol. 25, no. 2, pp. 485–520, 2011.
- [29] W. A. Smith and R. B. Randall, "Rolling element bearing diagnostics using the case western reserve university data: A benchmark study," *Mechanical systems and signal processing*, vol. 64, pp. 100–131, 2015.
- [30] N. Wang and X. Liu, "Bearing fault diagnosis method based on hilbert envelope demodulation analysis," in *IOP Conference Series: Materials Science and Engineering*, vol. 436, no. 1. IOP Publishing, 2018, p. 012009.